Article

A Fast and Accurate Prediction of Distortions in DCT-based Lossy Image Compression

Victoriya Abramova [1], Vladimir Lukin [1], Sergey Abramov [1], Sergii Kryvenko [1], Piotr Lech [2], and Krzysztof Okarma [2,*]

[1] Department of Information and Communication Technologies, National Aerospace University, 61070 Kharkiv, Ukraine; v.abramova@khai.edu (V.A.); v.lukin@khai.edu (V.L.); s.abramov@khai.edu (S.A.); krivenkos@ieee.org (S.K.)

[2] Department of Signal Processing and Multimedia Engineering, West Pomeranian University of Technology in Szczecin, Sikorskiego 37, 70-313 Szczecin, Poland; piotr.lech@zut.edu.pl (P.L.)

* Correspondence: okarma@zut.edu.pl

Abstract: Since the number of acquired images and their size have the tendency to increase, their lossy compression is widely applied for their storage, transfer, and dissemination. Simultaneously with providing a relatively large compression ratio, lossy compression produces distortions that are inevitably introduced and have to be controlled. The properties of these distortions depend on several factors such as image properties, the coder used, and a parameter that controls compression, which is different for particular coders. Then, one has to set a parameter that controls compression individually for an image to be compressed to provide image quality appropriate for a given application and it is often desired to make this quickly enough. Iterative procedures are usually not fast enough and therefore fast and accurate procedures for providing a desired quality are needed. In the paper, such a procedure for two coders based on Discrete Cosine Transform is proposed. This procedure is based on a prediction of Mean Square Errors for a given quantization step using a simple analysis of image complexity (local activity in blocks). The statistical and spatial-spectral characteristics of distortions introduced by DCT-based coders are analyzed and it is shown that they depend on the quantization step and local content. Generalizing the data for sets of grayscale test images and quantization step values, it is shown that MSE can be easily predicted. These predictions are accurate enough and can be used to set the quantization step properly as verified by experiments performed using several remote sensing and conventional optical images. The proposed approach is applicable to lossy compression of grayscale images and component-wise compression of multichannel data.

Keywords: lossy compression; DCT-based coders; Mean Square Error; statistical and spatial correlation analysis

Citation: Abramova, V.; Lukin, V.; Abramov, S.; Kryvenko, S.; Lech, P.; Okarma, K. A Fast and Accurate Prediction of Distortions in DCT-based Lossy Image Compression. *Electronics* **2023**, *1*, 0. https://doi.org/

Received:
Revised:
Accepted:
Published:

1. Introduction

A tremendous number of images of different origins are acquired nowadays. Ordinary customers acquire a huge number of color photos and put them into the Internet [1]. Numerous remote sensing (RS) spaceborne and airborne imagers acquire a lot of images each day [2,3]. Medical diagnostic complexes provide medicians with several types of image data [4], Internet shops and other services use advertising images [5], and so on.

Images acquired by the aforementioned systems have various properties, but there are common tendencies for them. Firstly, their number rapidly grows [6,7]. Secondly, the average size of images increases as well. Color photos become larger due to better digital cameras; a better spatial resolution as well as the use of multichannel imaging mode leads to a larger size of remote sensing images; the size of medical images has the tendency to increase, too. Then, to transfer, store and disseminate such images, data compression should be used. Lossless compression techniques are mostly unable to ensure a desired compression ratio (CR) [8–10]. Moreover, lossy image compression methods are able to produce considerably larger CRs that can be varied using a parameter that controls compression (PCC) [11–14]. This can be a quality factor (QF) used in JPEG [11], bits per pixel (BPP) employed in JPEG2000, quantization step (QS) utilized in DCT-based coders [13], Q-parameter in Better Portable Graphics (BPG) coder [14], etc. A general tendency that is valid for most images is that a larger CR (associated with a smaller QF or BPP or a larger QS or Q) results in a larger degradation and worse quality according to any metric, conventional or visual quality one [11–14]. Then, it is needed to find an appropriate compromise between the introduced distortion (quality of a compressed image) and CR for a given application and an image to be compressed [2,3,15].

Depending on the application, this compromise (and imposed restrictions) can be different. Some examples are the following:

1. Ensure CR as large as possible with simultaneous providing of acceptable visual quality; in this sense, two tasks have to be solved:
    - to find a coder that provides a larger CR for a given image and a given quality;
    - to find such a CR that distortions do not exceed the chosen threshold according to a considered quality metric;
2. Provide that (diagnostically) valuable information is not lost under the attempt to increase CR for a chosen coder;
3. Carry out lossy compression with simultaneous provision of acceptable quality as quickly as possible or within a certain time interval for a chosen coder and a quality metric threshold.

To solve the aforementioned tasks of reaching an acceptable compromise, one has to answer many questions including the following:

- What quality metric to use?
- What are metric values (thresholds) that correspond to the appropriateness of introduced distortions? With what accuracy should they be provided?
- How to compare the performance of compression techniques and what are good coders nowadays?
- What are the existing procedures for providing the desired quality, and what are their advantages and drawbacks?

A metric to be used should satisfy several requirements. In particular, it has to be adequate for a given application, its properties have to be thoroughly studied, and it should be calculated quickly enough. Mean Square Error (MSE) is one such metric. Its calculation is very fast, and MSE properties (in particular, with application to lossy image compression) are studied well. In particular, the Spearman correlation for MSE and Mean Opinion Score (MOS) for three subsets of images with distortions dealing with lossy compression in the database TID2013 [16] is equal to 0.914 and it is better than the correlation of SSIM [17] and MOS (0.893) but worse than for MOS and some modern visual quality metrics. Thus, MSE is quite an adequate metric for compressed images. It is also known that if distortions are similar to additive white Gaussian noise, then they are practically invisible for noise variance about 20 and less (for images represented by 8-bit data), i.e. for Peak Signal-to-Noise Ratio (PSNR) of about 35 dB and more [8]. MSE changes (differences) by $10 \ldots 20\%$ can be very hardly noticed in compressed images by visual inspection. Hence, in fact, the first two questions have been answered.

The performance of image compression techniques is usually analyzed by exploiting rate/distortion curves, i.e. dependences of a parameter that characterizes image quality on PCC or CR. To get correct conclusions, such an analysis has to be performed for quite many images and for a wide range of CR (PCC, image quality). The results of performance analysis carried out for several compression techniques [8,9,13] show that lossy compression techniques based on orthogonal transforms including DCT [10,11,14] provide good results. Some DCT-based coders sufficiently outperform the JPEG and JPEG2000 [12] standards. Since they are based on DCT, they can be easily incorporated into existing software and hardware image processing tools including on-board systems and devices of remote sensing image compression [18]. Because of this, the analysis below is concentrated on the prediction of MSE for the coders AGU [19] and ADCT (advanced DCT) [20] assuming that the proposed approach can be useful for other DCT-based compression techniques.

The paper structure is as follows. In Section 2 related work is discussed whereas Section 3 briefly describes the considered compression techniques and analyzes the existing solutions for MSE prediction. Statistical and spatial correlation analysis of distortions introduced by lossy compression is carried out in Section 4. Dependencies of statistical characteristics of distortions on image local activity are studied in this Section as well. A method for MSE prediction and its accuracy analysis are presented in Section 5. Finally, the conclusions follow in Section 6.

2. Related work

The problem of providing desired values of MSE (as well as other metrics) has been earlier considered in several papers [13,21–26]. Three main approaches are the following.

Firstly, an iterative procedure presuming multiple image compression/decompression with quality metric (e.g., MSE) estimation and PCC refining at each iteration can be used [13]. The advantage of such a procedure is that it is able to ensure a high accuracy of providing a desired value of a considered metric [13], e.g., PSNR with accuracy less than 0.2 dB (MSE with relative error less than 6%). The drawback is that the number of iterations is unknown in advance and, because of this, the requirements imposed on maximal time of compression can be sometimes not satisfied. In addition, the approach needs more computations than other two methods and, thus, it is not attractive from the viewpoint of green technologies [27].

Secondly, the so-called two-step procedures have been developed recently [23,28]. They are based on obtaining an average rate-distortion curve for a given coder (for example, MSE or PSNR on QS) in advance (off-line). This curve is then used to determine a starting point (initial QS) for image compression, decompression and metric calculation. Then, using the average curve derivative, the final QS is calculated, and the final compression is carried out. This approach is, on the average, considerably faster than iterative. However, its accuracy is worse compared to iterative approach and, in some situations such as quite large CR, can be inappropriate for practice. Besides, two compression steps and one decompression are needed in any case. This can be acceptable if both compression and decompression are fast enough but can make problems if either compression or decompression are not fast.

Thirdly, several approaches that can be treated as prediction based ones have been put forward [22,24–26,29]. Their main advantage is that they determine PCC (QS) based on prediction of metric value. Due to this, no preliminary compression and decompression as for the two-step approach are needed. This allows determining PCC quite quickly. In addition, for the approach [29], spatial distribution of distortions introduced by lossy compression can be predicted that can be useful for several goals of further image processing. However, the prediction accuracy is usually worse than for iterative and two-step approaches and its careful analysis has not been carried out.

Therefore, the goal of this paper is to further advance the approach proposed in our paper [29]. The novelty of this paper consists in two items. Firstly, the spatial distributions of introduced distortions are analyzed. Secondly, the statistical analysis of MSE predictions for a set of test grayscale images is carried out, including those images not used in obtaining the prediction curves.

3. Description of the Used Coders, Test Images and Preliminary Analysis of Compression Characteristics

3.1. Used Coders and Test Images

The most known and widely used DCT-based coder is JPEG [30]. Its positive and negative features are well known. In particular, the main drawbacks are the blocking effect and the use of fixed size blocks that limits potential of compression. These drawbacks

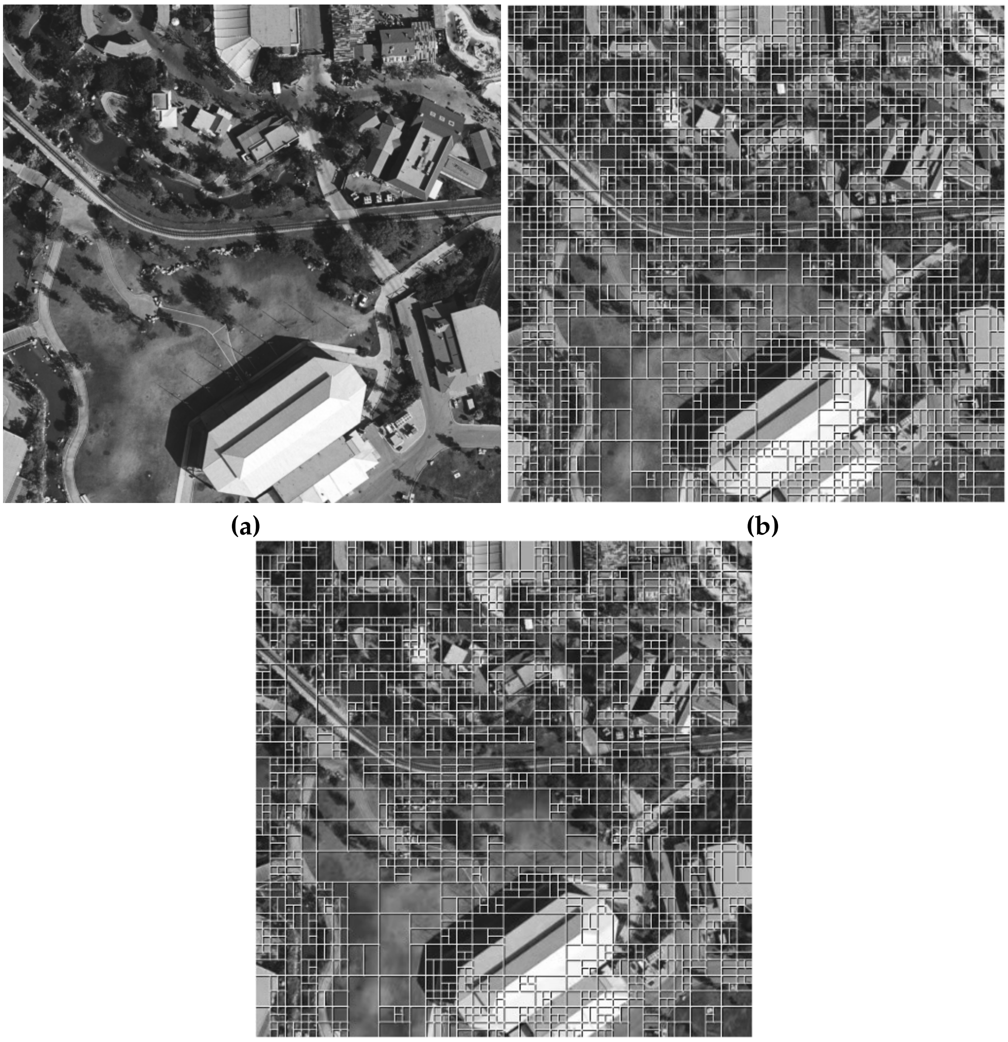

(a) **(b)** **(c)**

Figure 1. Illustration of the partition schemes: (**a**) Test image Fr01 and partition schemes for (**b**) QS=5, and (**c**) QS=20.

stimulated the studies intended on fuller exploitation of DCT potential in image and video compression applications. One of extensions is the AGU coder [19] based on the 2D DCT in 32×32 pixel blocks. In addition, AGU employs an efficient bit plain coding of the DCT coefficients after uniform quantization and decompressed image deblocking. Due to the aforementioned modifications, the AGU coder outperforms JPEG [30], SPIHT [31], JPEG2000 [12] as well as many other compression techniques [13].

Another compression technique considered in our study is ADCT coder (ADCTC) [20]. It attempts to avoid the drawback of using fixed block size (inherent for JPEG and AGU) by exploiting partition scheme optimization to adapt the block size to image content. An example is presented in Figure 1 where partition schemes are demonstrated for two QS values for one of test images. The blocks have square or rectangular shape where the side sizes are powers of 2 to provide an opportunity to use fast algorithms of DCT. The block sizes are larger for more homogeneous regions of images. The partition scheme is not the same for a given image, it changes with QS becoming slightly simpler if QS and CR increases.

The ADCTC requires more computations compared to JPEG and AGU, especially at compression stage when partition scheme has to be optimized. Decompression is faster than compression.

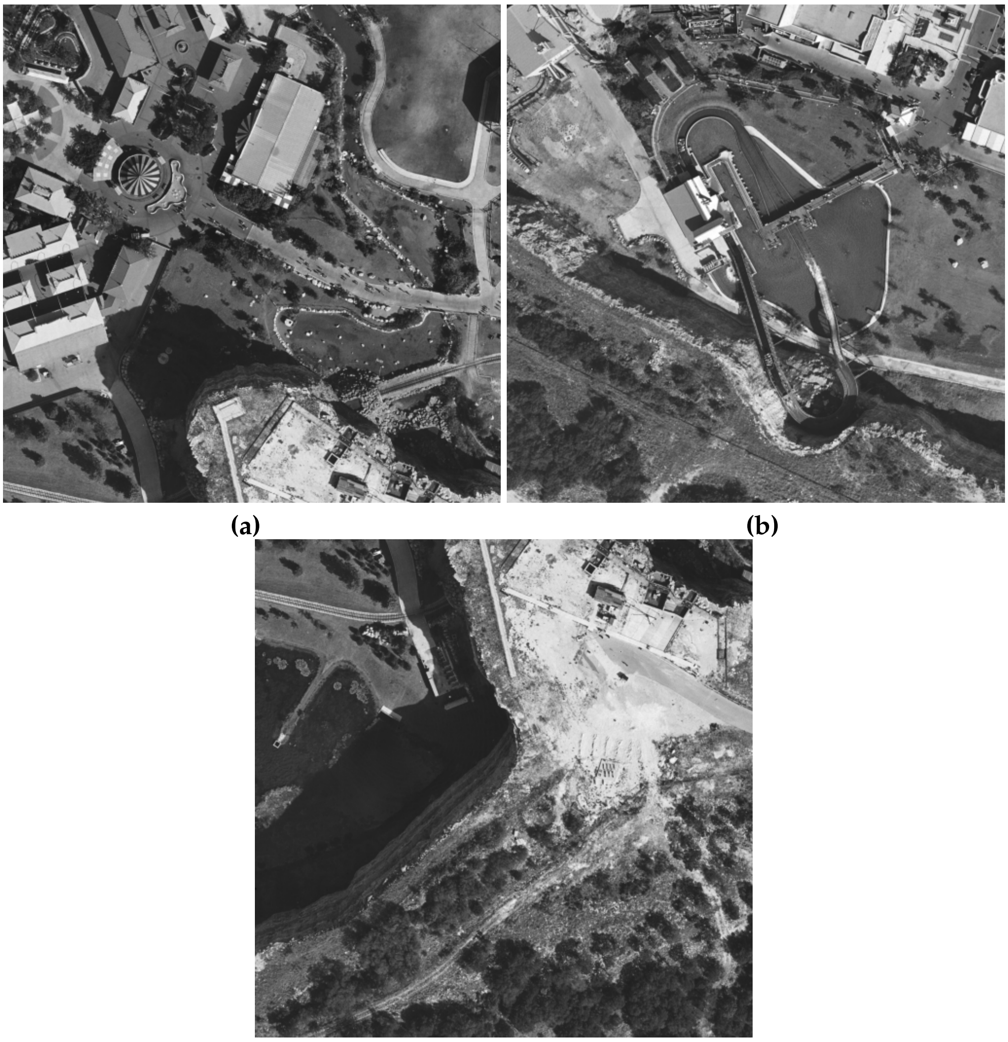

(a) **(b)**

(c)

Figure 2. Test images used in experiments: Fr02 (**a**), Fr03 (**b**), Fr04 (**c**).

At preliminary stage of our studies, in addition to the test image in Figure 1a, the three other test images given in Figure 2 have also been employed. These are typical remote sensing images of natural scenes of a medium complexity.

All images are of the size 512 $\times$ 512 pixels allowing the use of coders' versions freely available at https://ponomarenko.info/agu.htm and https://ponomarenko.info/adct.htm. Note that an interested reader can find some performance comparison results there.

3.2. Preliminary Analysis of Some Rate/Distortion Characteristics

Recall that our analysis is mainly focused on practical situations when compression is visually lossless or, at least, the introduced distortions are not annoying. This happens if PSNR is about 35 dB (let us say, from 30 to 45 dB) [32]. As said above, PSNR is not the best metric if the goal is to adequately characterize the visual quality of compressed images. Hence, the visual quality metric PSNR-HVS-M [33] should be considered as well. It takes into account two important peculiarities of human vision system (HVS) and its properties have been thoroughly studied in [32]. Similarly to PSNR, PSNR-HVS-M is expressed in dB. The properties of PSNR-HVS-M important for our further analysis are the following. The values of PSNR-HVS-M are larger compared to the values of the corresponding PSNR if distortions' properties are similar to the properties of additive white Gaussian noise (AWGN) and a considered image is able to mask noise (distortions), at least partially (this happens if a distorted image has texture fragments are quite many fine details). One

Table 1. Characteristics of test image compression for AGU.

Parameter	QS = 5	QS = 10	QS = 20
		Image Fr01	
bpp	3.24	2.29	1.40
PSNR [dB]	45.06	39.74	34.75
PSNR-HVS-M [dB]	55.20	47.31	39.71
		Image Fr02	
bpp	3.28	2.34	1.46
PSNR [dB]	45.13	39.77	34.71
PSNR-HVS-M [dB]	54.98	47.46	39.87
		Image Fr03	
bpp	3.32	2.37	1.46
PSNR [dB]	44.97	39.53	34.45
PSNR-HVS-M [dB]	55.48	47.31	39.55
		Image Fr04	
bpp	3.09	2.19	1.35
PSNR [dB]	45.21	39.85	34.71
PSNR-HVS-M [dB]	54.28	47.11	39.63

more important property is that distortions are visible if PSNR-HVS-M does not exceed 41 dB [32].

Let us start our analysis from the coder AGU and consider the following three values of QS equal to 5, 10, and 20. Table 1 contains the following parameters: bpp (bits per pixel) that can be recalculated from CR as bpp = 8/CR (for grayscale images represented as 2D 8-bit data arrays), PSNR, and PSNR-HVS-M.

As seen, the case of QS = 5 can be associated with near lossy compression since for all four test images the bpp values are slightly larger than 3, PSNR values are sufficiently larger than 35 dB, and PSNR-HVS-M values exceed 55 dB. The case of QS=20 relates to visible distortions which are not annoying distortions. For QS = 20, bpp is about 1.4, i.e. CR exceeds 5. Since PSNR values are slightly smaller than 35 dB and PSNR-HVS-M values are of about 39.7 dB for all four test images, distortions can be noticed by visual inspection. The case of QS = 10 can be treated as intermediate: CR is of about 3.5, PSNR is of about 39.7 dB, and PSNR-HVS-M is of about 47.3 dB, i.e. distortions are not visible. The presented examples are in good agreement with the results in our paper [13], where it is shown that, on the average, QS has to be set equal to 16 to provide invisibility of introduced distortions for both considered coders.

From data in Table 1, it might seem that the values of PSNR, PSNR-HVS-M and bpp (CR) for a given QS are almost the same and it is not a problem to provide a desired quality.

However, it is not true (the reason of approximate coincidence of performance characteristics for the considered four test images is that their complexity is similar). In [13], it is shown that, e.g., for bpp = 1.6, PSNR-HVS-M values vary in the limits from 30 dB to 53 dB. It is also shown in [23] that PSNR values for the same QS can differ by up to 10 dB (for QS of about 20).

Let us now briefly consider preliminary data for ADCTC. They are presented in Table 2 where the values of CR/bpp and MSE/PSNR for four test images and three values of QS are given. As it may be seen, the main tendencies are the same:

- CR increases (bpp reduces) if QS increases;
- MSE increases (PSNR reduces) if QS becomes larger;
- MSE increases almost proportionally to QS^2, hence the obtained value for QS = 5 is

$$MSE \approx \frac{QS^2}{12} \, . \tag{1}$$

Table 2. Characteristics ot test image compression for ADCTC.

Image	QS	CR	bpp	MSE	PSNR
Fr01	5	2.19	3.01	2.08	44.95
Fr02	5	2.65	3.03	2.03	45.06
Fr03	5	2.53	3.18	2.10	44.91
Fr04	5	2.74	2.93	1.98	45.16
Fr01	10	3.97	2.02	7.34	39.47
Fr02	10	3.87	2.08	7.13	39.60
Fr03	10	3.71	2.17	7.71	39.26
Fr04	10	3.98	2.02	7.03	39.66
Fr01	20	6.78	1.18	23.03	34.51
Fr02	20	6.46	1.24	23.17	34.48
Fr03	20	6.37	1.26	25.38	34.09
Fr04	20	6.73	1.19	23.92	34.34

(a) **(b)**

Figure 3. Noise-free test images “Frisco” (**a**) and “Airfield” (**b**).

Meanwhile, for QS = 10, MSE = 8.33 is already noticeably less than $QS^2/12$, and for QS = 20 this difference further increases (as 400/12 ≈ 33.33). Moreover, true MSE becomes quite different for the considered test images.

A quite thorough analysis of the observed tendencies and reasons for them has been carried out in [24]. Further, some interesting dependencies from this paper are presented, considering two noise-free and one noisy images. The noise-free images are “Frisco” and “Airfield” presented in Figure 3a and Figure 3b, respectively. As one can see, the image “Frisco” contains many quasi-homogeneous regions and, thus, it can be treated as simple structure one. Moreover, “Airfield” is approximately of the same complexity as the test images in Figure 2. The third considered image is the same test image “Frisco_std5” but with the artificially generated additive white Gaussian noise (AWGN) with zero mean and noise variance equal to 25. The purpose for considering such an image was to analyze noise influence on compression characteristics.

Dependencies of MSE determined between the compressed image and the corresponding image before compression for the ADCTC are presented in Figure 4. Although for all three test images MSE increases if QS becomes larger, there are sufficient differences. Firstly, MSE for the noise-free image “Frisco” is always the smallest and, for QS starting from 10, it is smaller that for two other test images by several times. For QS = 20, MSE for the noise-free test image is smaller than $QS^2/12$ by about 5 times, i.e. by about 7 dB. Secondly, till QS = 17, the curves for the test images noisy “Frisco_std5” and noise-free “Airfield” practically coincide and the approximate expression (1) is practically valid. However, for

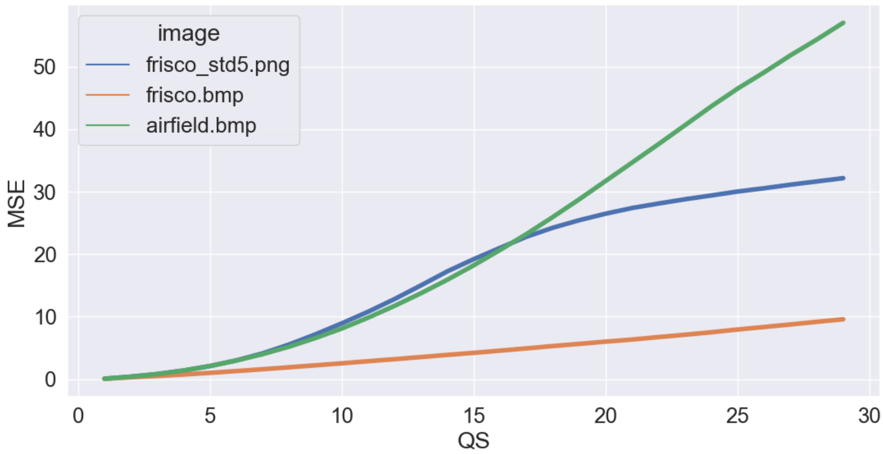

Figure 4. Dependencies of MSE on QS for ADCTC determined for three test images.

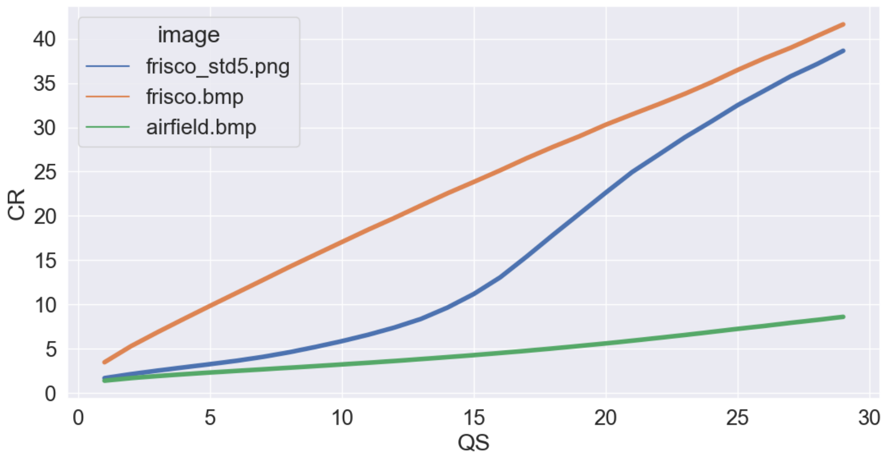

Figure 5. Dependencies of CR on QS for ADCTC determined for three test images.

a larger QS, the curves behave in a different manner. Thirdly, depending on noise variance, dependencies are considerably different even for images of the same content ("Frisco" and noisy "Frisco_std5"). This example shows that noise sufficiently influences coder performance.

The latter conclusion is also confirmed by the plots in Figure 5 that show dependencies of CR on QS for ADCTC for the considered three images. CR for the simple structure noise-free image "Frisco" is sufficiently larger than for the test image "Airfield" and noisy image "Frisco_std5". Only for quite large QS (i.e., QS = 25), CR values for compressed noise-free and noisy images ("Frisco" and "Frisco_std5") become close and this happens due to noise-filtering effect observed for lossy compression of noisy images.

Differences in the dependencies in Figures 4 and 5 are explained in [24] in detail where it is shown that distributions of DCT coefficients differ significantly for the considered three images and parameters of these distributions (e.g., percentage of DCT coefficients that become zero after quantization) are in a rather strict connection with MSE and CR. Meanwhile, the main goal of the analysis above was to demonstrate variability of MSE for the same QS and coder depending on the image complexity and the presence of noise. At the same time, the presented results can be treated as the background of the idea that MSE can be predicted for a given QS if an image to be compressed is somehow quickly analyzed to determine its main properties. Thus, let us briefly recall the existing approaches and solutions.

The paper [21] was probably the first interesting attempt to predict MSE and PSNR for the JPEG coder. The authors have assumed that distribution of AC DCT coefficients in 8×8 pixel blocks is close to Laplacian. Thus, by estimating the distribution scale S and using the a priori obtained dependence of MSE on QS/S, it is possible to predict MSE. However, there are two drawbacks of this approach. Firstly, the authors of [21] have proposed to perform scale estimation for AC DCT coefficients calculated in all blocks of an image planned to be compressed. This means that the first stage (obtaining DCT coefficients) in 8×8 pixel blocks takes the same time and the first stage of compression itself. Thus, prediction is not faster than compression or time expenses are of the same order. The second drawback is that distribution of AC DCT coefficients can differ from Laplacian. This leads to prediction errors that might exceed 1 dB.

If one deals with the AGU and ADCT coders, prediction should be considerably faster than compression. Based on the results in [21], two ways to better predict MSE for advanced DCT-based coders [22,24–26] have been put forward. The main ideas in the papers [25,26] are two-fold. Firstly, it is possible to predict MSE by processing original and quantized DCT coefficients in 8×8 pixel blocks with recalculating (correcting) the predictions for AGU and ADCT coders. Secondly, it is not necessary to consider all the possible block positions — it is enough to analyze 500–1000 randomly chosen blocks. The predictions are quite accurate, but DCT is still needed to be done for quite many blocks.

Another approach [22,24] is based on using the following expression:

$$MSE_{pred} = \frac{QS^2}{12} \cdot f(X) \, , \tag{2}$$

where $f(X)$ is a function of one or several parameters that describe the properties of an image to be compressed (its complexity or simplicity, the presence and amount of noise, etc.). In the simplest case, X is the aforementioned percentage of AC DCT coefficients that become zero after quantization. The drawbacks of this approach are the two-fold. Firstly, it is anyway needed to estimate statistics of DCT coefficients, i.e. to apply DCT. Secondly, the method's accuracy is not high if the percentage exceeds 0.8, i.e. for quite large QS (e.g. QS = 20).

Therefore, it is desirable to develop a technique that provides accurate prediction without applying DCT (and faster than existing techniques). It is also desired to utilize a rather accurate and universal method where the universality is considered its appropriate performance for a wide set of images and QS values.

4. Detailed Analysis of Distortion Properties

The necessity to study statistical and spatial-spectral properties of distortions introduced by different coders is significant for several reasons. Firstly, it has been stated in [34] that the distortions due to lossy compression have to be of limited intensity and have spatially "uniform" distribution to avoid artifacts (including classification artifacts). Secondly, the results in [26] have demonstrated that the distortions have a distribution close to Gaussian for relatively small CR and QS for complex structure images whereas the distribution might be non-Gaussian for simple structure images. However, the reasons for this have not been explained. Because of this, it is worth recalling the data recently presented in our paper [29] where the visual and quantitative analysis of difference images has been performed. Note that difference images are quite often used in analysis of image lossy compression and denoising. Let $\{I^{or}(i,j), i = 1, \ldots, I_{Im}, j = 1, \ldots, J_{Im}\}$ be an original image having the size of $I_{Im} \times J_{Im}$ pixels and $\{I^{c}(i,j), i = 1, \ldots, I_{Im}, j = 1, \ldots, J_{Im}\}$ represent the corresponding compressed image. In simulations, both images are available and the difference image can be calculated as

$$\{\Delta(i,j) = I^{or}(i,j) - I^{c}(i,j), i = 1, \ldots, I_{Im}, j = 1, \ldots, J_{Im}\} \, . \tag{3}$$

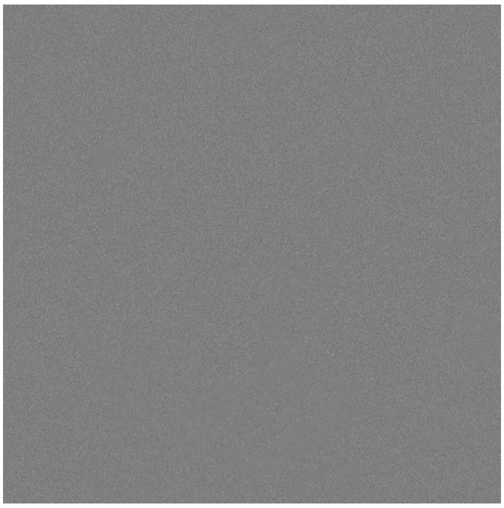

Figure 6. Difference image Δ_p for the compressed image Fr01 for QS = 20.

Table 3. Mode of local kurtosis estimates.

Image	QS = 5	QS = 10	QS = 20
Fr01	2.6974	2.7507	2.8896
Fr02	2.7189	2.7642	2.9065
Fr03	2.7192	2.7446	2.8437
Fr04	2.7573	2.7933	2.8510

In most practical situations, $\Delta(i,j)$ are integers that can be negative, positive and equal to zero.

For visual inspection, there are several ways to present difference images, e.g.:

- as absolute values of differences (including preliminary magnification);
- using the pedestal, for example, as

$$\{\Delta_p(i,j) = I^{or}(i,j) - I^{c}(i,j) + 128, i = 1,\ldots,I_{Im}, j = 1,\ldots,J_{Im}\}\ .$$

One example of $\{\Delta_p(i,j), i = 1,\ldots,I_{Im}, j = 1,\ldots,J_{Im}\}$ is presented in Figure 6 for the test image Fr01 compressed by AGU with QS = 20. The fluctuations (distortions) can be hardly noticed since PSNR is about the distortion visibility threshold (slightly smaller than 35 dB). The visualized distortions are absolutely not seen for QS = 5 and QS = 10. Because of this, the difference images are not shown here.

Since it is expected that differences (3) can be a non-stationary 2D process, its spatial spectral or correlation analysis should be performed with care. One methodology of such an analysis applicable for signal-dependent or spatially invariant data has been proposed in [35,36]. One has to determine the mode of local kurtosis estimates obtained in DCT domain. If this mode is smaller than 3.75, the noise can be assumed spatially uncorrelated.

The obtained results are presented in Table 3. As one can see, the distortions can be considered spatially uncorrelated for all four test images and all three QS values. However, one can observe a tendency to mode increasing (i.e. to a larger spatial correlation of distortions) when QS increases.

Similar analysis has been carried out for the ADCT coder. The results are practically the same — the distortions can be considered spatially uncorrelated, at least, for QS $\leq$ 20.

Let us carry out statistical analysis in blocks keeping in mind possible non-stationarity of distortions. Let us employ non-overlapping 8×8 pixel blocks and calculate in each of them the following two parameters (where each block position is defined by the left upper corner coordinates n and m:

$$\sigma^2_{dist} = \frac{1}{64} \cdot \sum_{i=m}^{m+7} \sum_{j=j}^{n+7} \left(\Delta_p(i,j) - \overline{\Delta}\right)^2 , \quad (4)$$

$$\sigma^2_{im} = \frac{1}{64} \cdot \sum_{i=m}^{m+7} \sum_{j=j}^{n+7} \left(I^{or}(i,j) - \overline{I^{or}}\right)^2 , \quad (5)$$

where $\overline{\Delta} = \frac{1}{64} \cdot \sum_{i=m}^{m+7} \sum_{j=j}^{n+7} \Delta_p(i,j)$ and $\overline{I^{or}} = \frac{1}{64} \cdot \sum_{i=m}^{m+7} \sum_{j=j}^{n+7} I^{or}(i,j)$.

It is possible to present the obtained data as scatter-plots of Root Mean Square Error (RMSE) of distortions σ_{dist} vs RMSE of σ_{im} characterizing noise local (content) activity. For the test image Fr01, the obtained scatter plots are given in Figure 7 for three values of QS. Their analysis shows the following:

1. One can observe large areas of σ_{im} where σ_{dist} are, in general, random, but their mean is practically constant; later such areas will be called the saturation ones;
2. Not surprisingly, in such areas, mean σ_{dist} is approximately equal to $(QS^2/12)^{0.5}$ — about 1.4 for QS = 5 (Figure 7a), about 2.7 for QS = 10 (Figure 7b), and about 5 for QS = 20 (Figure 7c);
3. If σ_{im} is quite small, there is the tendency of σ_{dist} decrease (on average) with a reduction of σ_{im}; this tendency may be observed when $\sigma_{im} \leq QS$.

The scatter plots obtained for the other three test images are very similar to those represented in Figure 7. To illustrate this, the scatter plots for the test image Fr02 are given in Figure 8. As it may be seen, the conclusions that can be drawn from their analysis, are the same as given above.

Having obtained such scatter plots, it is possible to carry out regression, i.e. to fit the curves. For this purpose, the following approximation is used:

$$\sigma^{appr}_{dist} = a \cdot \exp(b \cdot \sigma_{im}) + c , \quad (6)$$

where a, b, and c are the function parameters to be estimated. For curve fitting and estimation of its parameters, MATLAB *fminsearch* function may be used, which allows to find a minimum of unconstrained multi-variable function using derivative-free method.

The parameters of the fitted curves are given in Table 4. For the same QS, the parameter values of the fitted curves for the considered test images are very similar. This especially relates to the parameter c that describes the "saturation level".

Table 4. Parameters of the fitted curves (AGU).

Image	QS = 5	QS = 10	QS = 20
Fr01	$a = -0.50$ $b = -0.40$ $c = 1.44$	$a = -1.37$ $b = -0.25$ $c = 2.73$	$a = -3.41$ $b = -0.13$ $c = 5.21$
Fr02	$a = -0.91$ $b = -0.57$ $c = 1.44$	$a = -2.04$ $b = -0.33$ $c = 2.74$	$a = -4.03$ $b = -0.16$ $c = 5.24$
Fr03	$a = -0.74$ $b = -0.63$ $c = 1.44$	$a = -1.28$ $b = -0.25$ $c = 2.77$	$a = -3.35$ $b = -0.14$ $c = 5.31$
Fr04	$a = -1.01$ $b = -0.55$ $c = 1.45$	$a = -2.41$ $b = -0.33$ $c = 2.80$	$a = -4.97$ $b = -0.17$ $c = 5.46$

The presented scatter plots explain why MSE of distortions introduced by lossy compression into simple structure images differs from MSE of introduced distortions for com-

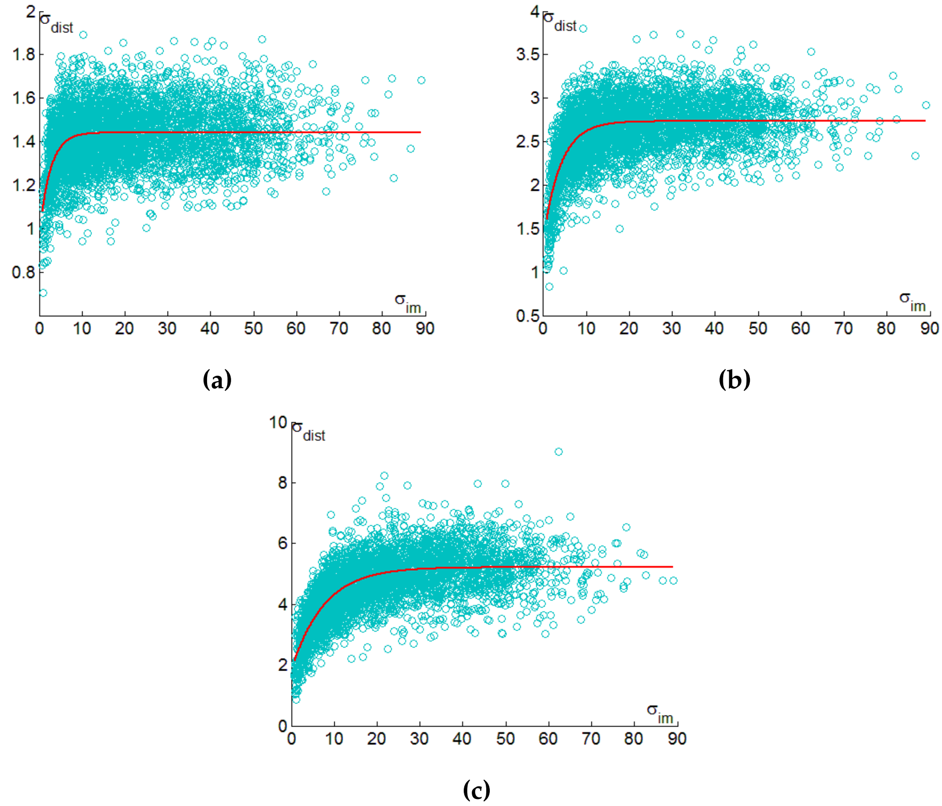

Figure 7. Scatter plots σ_{dist} vs σ_{im} for the test image Fr01 for QS equal to: 5 (**a**), 10 (**b**), and 20 (**c**).

plex structure images. Complex structure images mostly have the blocks where σ_{im} is large enough due to high local activity and then σ^2_{dist} for such blocks is, on average, approximately equal to $QS^2/12$. Then, MSE for entire image is close to $QS^2/12$ as well. Meanwhile, when QS increases, there are less blocks in the saturation area and MSE for entire image occurs to be smaller than $QS^2/12$.

Let us now present the scatter plots of σ_{dist} vs σ_{im} for the ADCT coder. They are given in Figure 9. It is possible to compare the scatter plots in Figure 9 to the corresponding scatter plots in Figures 7 and 8.

The comparison shows that the main properties of the scatter-plots are very similar. Again, there are saturation zones observed for $\sigma_{im} > Q$ where σ_{dist} are approximately equal to $(QS^2/12)^{0.5} = QS/3.47$. When $\sigma_{im} \leq Q$, then σ_{dist} decreases with a reduction of QS.

This reduction can be explained as follows. In quasi-homogeneous image regions (blocks), there is a large percentage of DCT coefficients that are smaller than QS (especially if QS is large enough). Quantization errors for such DCT coefficients, on average, have smaller absolute values compared to the case when most DCT coefficient have absolute values larger than QS (see the distributions of quantization errors in [21]). Since quantization errors in DCT domain are smaller, local MSEs for the corresponding blocks of compressed images are smaller as well.

The map of σ_{im} in blocks (magnified by 5 for better visualization) for the test image "Frisco" (Figure 3a) is presented in Figure 10a, whereas Figure 10b shows the map of σ_{dist} in blocks (magnified by 28 for better visualization) for the same test image. It is clearly seen that σ_{dist} is smaller (pixels are darker) in homogeneous regions of the image where the values of σ_{im} are smaller (the pixels are darker).

The scatter plots for other test images are very similar. The parameters of the fitted curves obtained using the approximation (6) are presented in Table 5. In comparison to the corresponding values in Table 4 they are very similar. The only difference is that the values of the parameter c for the ADCT coder are slightly larger. However, they are

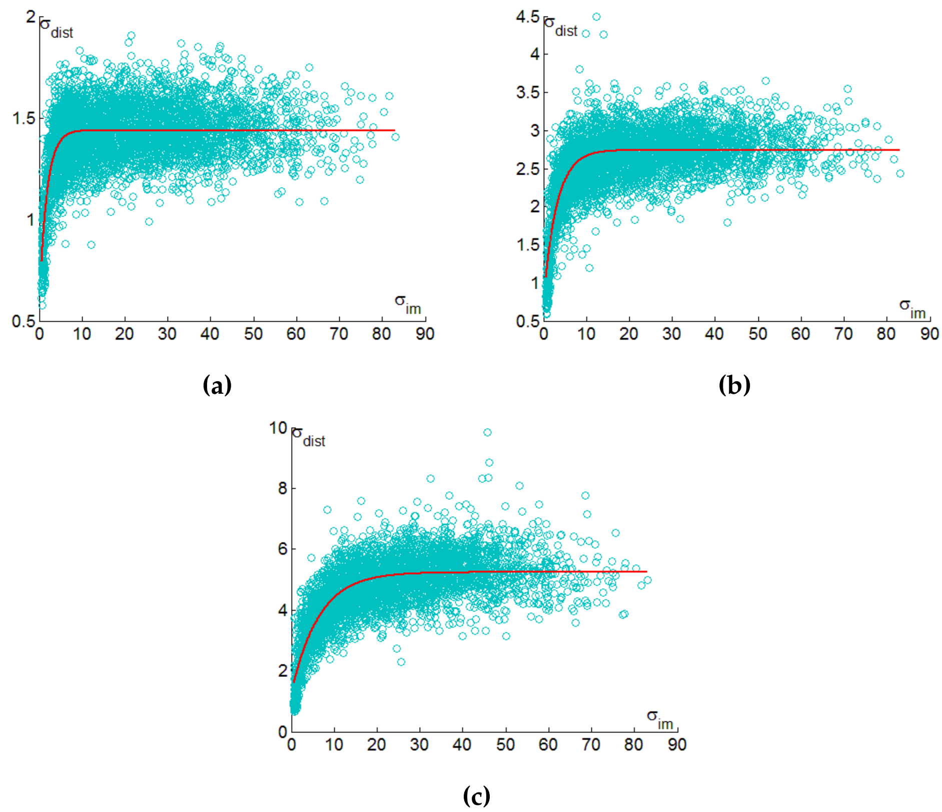

Figure 8. Scatter plots σ_{dist} vs σ_{im} for the test image Fr02 for QS equal to: 5 (**a**), 10 (**b**), and 20 (**c**).

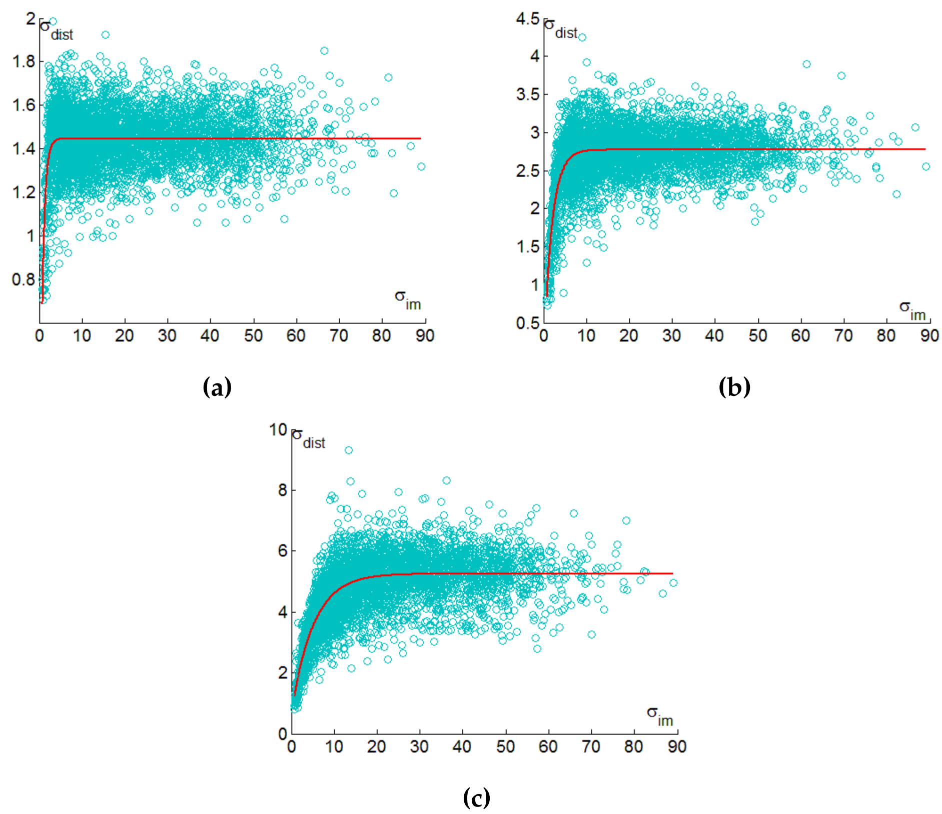

Figure 9. Scatter plots σ_{dist} vs σ_{im} for QS equal to: 5 (**a**), 10 (**b**), and 20 (**c**) for the test image Fr01 (ADCTC).

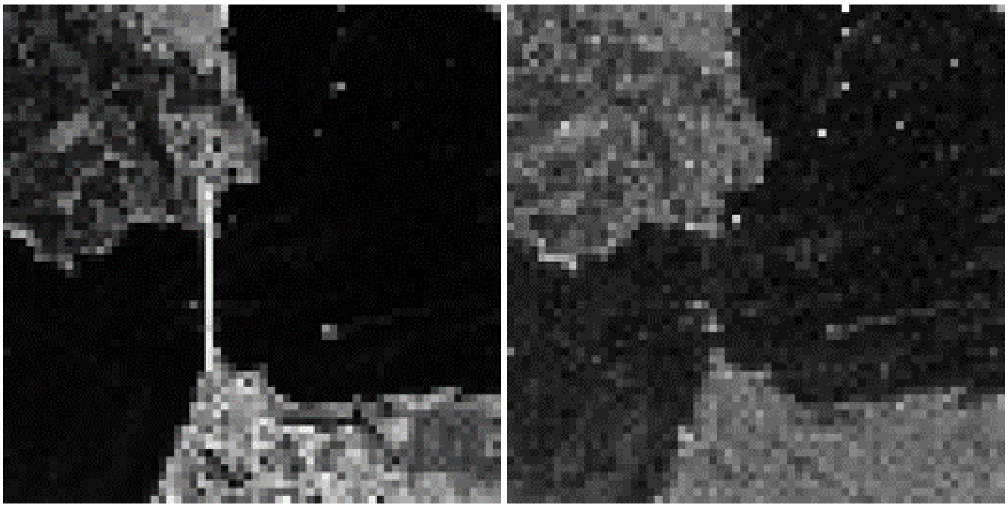

Figure 10. Maps of σ_{im} (**a**) and σ_{dist} (**b**) in blocks for the test image "Frisco".

Table 5. Parameters of the fitted curves (ADCTC).

Image	QS = 5	QS = 10	QS = 20
Fr01	$a = -2.42$ $b = -1.44$ $c = \ \ 1.45$	$a = -2.95$ $b = -0.52$ $c = \ \ 2.77$	$a = -4.69$ $b = -0.20$ $c = \ \ 5.25$
Fr02	$a = -1.59$ $b = -1.00$ $c = \ \ 1.45$	$a = -2.97$ $b = -0.50$ $c = \ \ 2.77$	$a = -5.17$ $b = -0.21$ $c = \ \ 5.33$
Fr03	$a = -2.86$ $b = -1.44$ $c = \ \ 1.45$	$a = -4.22$ $b = -0.74$ $c = \ \ 2.80$	$a = -4.96$ $b = -0.22$ $c = \ \ 5.40$
Fr04	$a = -1.35$ $b = -0.85$ $c = \ \ 1.45$	$a = -2.86$ $b = -0.43$ $c = \ \ 2.84$	$a = -5.59$ $b = -0.20$ $c = \ \ 5.64$

again approximately equal to QS/3.47 (1.44, 2.88, and 5.76 for QS equal to 5, 10, and 20, respectively).

Since a great number of σ_{dist} and σ_{im}, corresponding to each other, are obtained for three values of QS, it is possible to obtain aggregate scatter plots for both considered coders. Furthermore, the scatter plots in a normalized way as the dependence of $12^{0.5} \cdot \sigma_{dist}/QS$ vs σ_{im}/QS are presented. For the coder AGU, the aggregated scatter plot is presented in Figure 11. The general properties of this scatter plot are similar to those ones presented earlier. There is a monotonously increasing part of the fitted curve observed for $\sigma_{im}/QS < 1$ and the "saturation part" where $12^{0.5} \cdot \sigma_{dist}/QS$ is close to unity that takes the place for $\sigma_{im}/QS \geq 1$. The fitted curve is expressed as

$$f(\sigma_{im}/QS) = -0.7381 \cdot \exp(-2.8526 \cdot \sigma_{im}/QS) + 0.9685\,. \tag{7}$$

Note that the value of the parameter c is not equal to 1 but it is quite close to unity.

Similarly, the aggregated scatter plot has been obtained for the ADCT coder. It is presented in Figure 12. Comparison of the scatter plots in Figures 11 and 12 shows that their main properties are quite close. Note that large ratios σ_{im}/QS relate to "very active" local areas (where sharp edges or large contrast small-sized objects are observed) and quite small QS values.

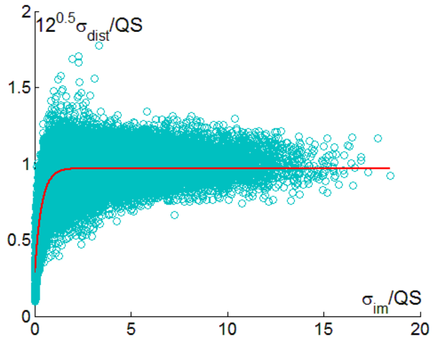

Figure 11. Aggregated scatter plot for different test images and QS values for the coder AGU.

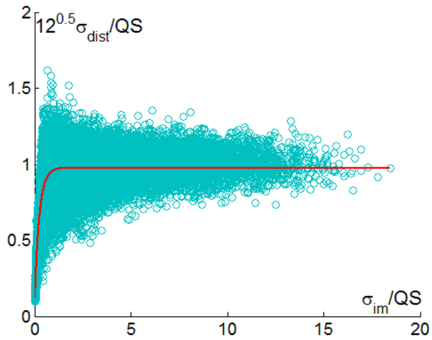

Figure 12. Aggregated scatter plot for different test images and QS values for the ADCT coder.

The largest variations of $12^{0.5} \cdot \sigma_{dist}/QS$ with respect to the fitted curves take place for $\sigma_{im}/QS \approx 1$. Such situations are observed for blocks that correspond to low contrast edges, details and textures that are the most typical for natural scene images.

The obtained fitted curve is given as

$$f(\sigma_{im}/QS) = -0.9498 \cdot \exp(-4.0992 \cdot \sigma_{im}/QS) + 0.9762\ . \tag{8}$$

In this case, the value of the parameter c is even closer to unity.

5. MSE Prediction and its Accuracy

Having obtained the expressions (7) and (8) for the AGU and ADCT coders, respectively, it is possible to predict σ_{dist} for each k-th 8×8 pixels block of a given image using the corresponding estimate σ_{im} obtained for this block.

For a given block and QS, one has

$$\sigma_{dist} \approx (QS/12^{0.5}) \cdot f(\sigma_{im}/QS)\ . \tag{9}$$

Assuming the knowledge of the estimates $\sigma_{dist}(k), k = 1, \ldots, K$ where K denotes the total number of blocks (the questions how the blocks can be positioned and what should be their number will be discussed later), the MSE for entire image can be predicted as

$$MSE \approx \sum_{k=1}^{K} \sigma^2_{dist}(k)/K \tag{10}$$

or

$$MSE \approx \sum_{k=1}^{K} \frac{QS^2}{12} \cdot f^2(\sigma_{im}(k)/QS)/K\ , \tag{11}$$

where $\sigma_{im}(k)$ is the value of RMSE in a k-th block determined by the formula (5). Note that it is very easy to calculate all $\sigma_{im}(k), k = 1, \ldots, K$ in advance if the block positions are known in advance as well.

Let us now analyze the accuracy of predicting MSE for introduced distortions. Table 6 presents the data for the four test images used in forming the scatter plots for the AGU coder. As it may be seen, the true values of MSE are close to the corresponding predicted ones (MSE_{pred}), the relative difference is considered small in practical applications as it does not exceed 10%. The data for the ADCT coder for the same four images are presented in Table 7. Their analysis shows that the true and predicted values are also quite close. The maximal difference does not exceed 8%, i.e. 0.3 dB with regard to PSNR.

However, the results for images that have not been used in training (obtaining the fitting curves for the scatter plots) are more interesting. Such verification data have been obtained for 16 other test images of different origins. There are some traditional images such as: "Lena", "Baboon", "Barbara", "Boat", "Goldhill", "Peppers", and "Man". There are also highly textural images as "Grass" and "Bikes" (see small copies in Figure 13). Several remote sensing images, such as "Frisco", "Airfield" (both shown in Figure 3), "Lu01", "San Diego1", "a13sm", "Sent01", "Sent02" (see small copies in Figure 13) have also been used. The goal of using images of different origins is to demonstrate that the proposed approach to prediction is applicable in different practical situations.

Selected results are presented in Tables 8 and 9 where the most interesting examples are shown. Alongside with this, statistical results characterizing the accuracy of prediction are presented below.

Analysis of data in Table 8 demonstrates the following. Firstly, for QS = 5, the MSE values do not differ significantly (they vary from 1.55 to 2.14) and they are predicted well. Secondly, for QS = 10, the difference in MSE values increases (they vary from 4.2 for simple structure image "Lu01" to 7.81 for the complex structure image "Grass"), but prediction still is considered accurate enough. Finally, for QS = 20, MSE may differ noticeably depending on image complexity (from 10.21 for "Lu091" to 30.92 for the test image "Grass"). However, predicted values are in good agreement with the true MSE and this happens for all images used in our analysis.

Bias and variance have been also determined for the true and predicted values for all twenty images used in analysis. For QS = 5, they are equal to -0.11 and 0.18; for QS = 10 — equal to 0.07 and 0.51; for QS = 20 — equal to 2.77 and 8.66, respectively. Bias and RMSE are smaller than 15% of mean values for each QS and such an accuracy is acceptable for practice (in fact, PSNR is predicted with maximal error less than 1.5 dB).

Analysis of data presented in Table 9 shows the following. Firstly, if QS = 5, the MSE values vary in rather narrow limits (from 1.69 to 2.14) and they can be predicted well enough. Secondly, when QS = 10, the MSE values vary from 4.61 for the image "Lu01" having simple structure to 8.21 for the image "Grass" with the complex structure. The

Table 6. Comparison of true and predicted MSE values for the AGU coder.

Image	QS	MSE	MSE_{pred}
Fr01	5	2.03	1.88
Fr02	5	1.99	1.85
Fr03	5	2.07	1.90
Fr04	5	1.96	1.78
Fr01	10	6.91	6.97
Fr02	10	6.85	6.85
Fr03	10	7.24	7.12
Fr04	10	6.74	6.55
Fr01	20	21.84	23.88
Fr02	20	21.95	23.67
Fr03	20	23.30	24.39
Fr04	20	22.02	22.24

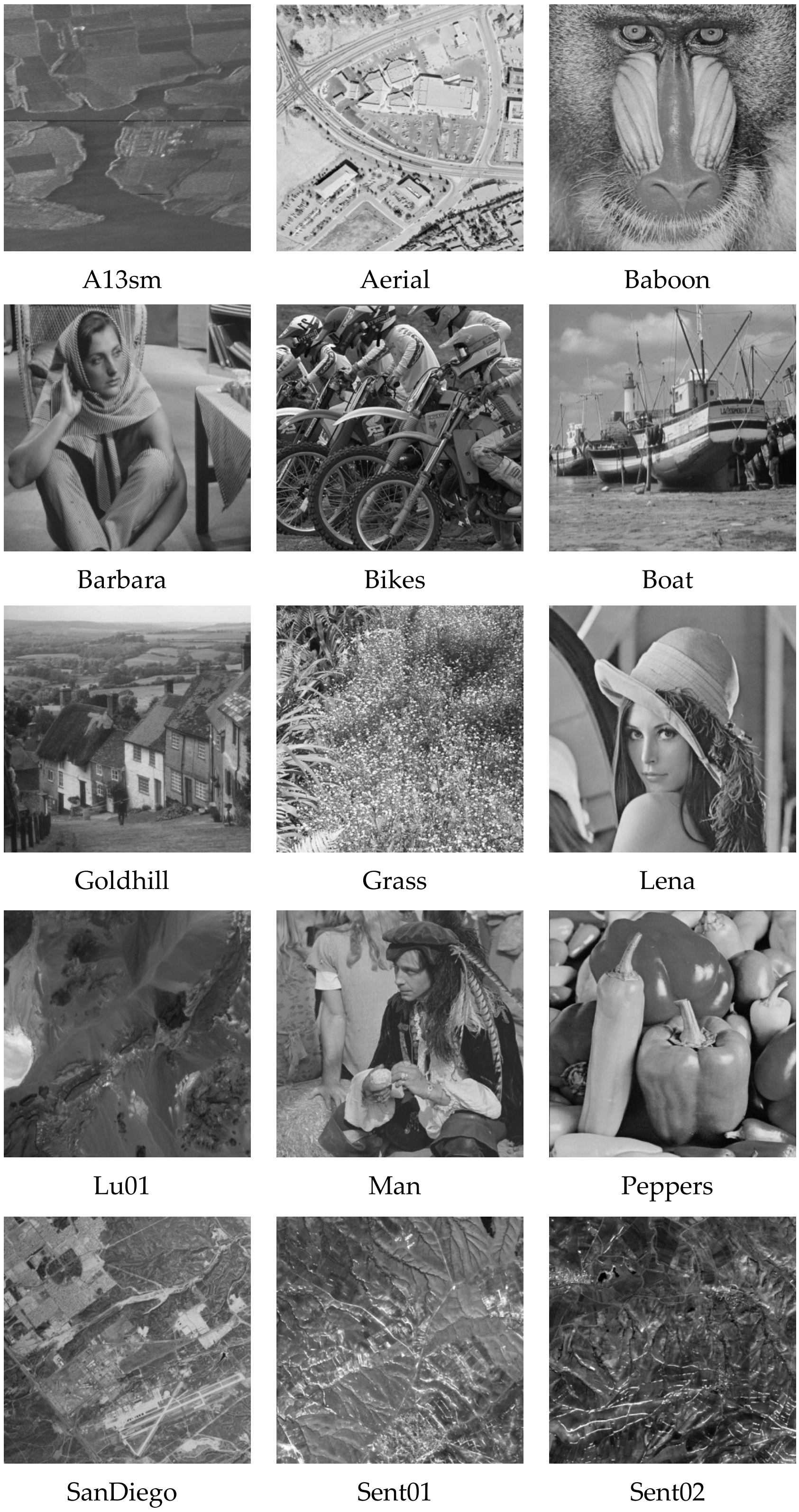

Figure 13. Small copies of test images used in experiments.

Table 7. Comparison of true and predicted MSE values for the ADCT coder.

Image	QS	MSE	MSE_{pred}
Fr01	5	2.08	1.94
Fr02	5	2.03	1.90
Fr03	5	2.10	1.95
Fr04	5	1.98	1.84
Fr01	10	7.34	7.30
Fr02	10	7.13	7.15
Fr03	10	7.71	7.45
Fr04	10	7.03	6.83
Fr01	20	23.03	25.51
Fr02	20	23.17	25.12
Fr03	20	25.38	26.23
Fr04	20	23.92	23.66

Table 8. Comparison of true and predicted MSE values for the AGU coder for sample images used during the experimental verification.

Image	QS	MSE	MSE_{pred}
A13sm	5	1.74	1.70
A13sm	10	5.53	4.87
A13sm	20	15.02	12.63
Grass	5	2.14	1.95
Grass	10	7.81	8.25
Grass	20	30.92	31.38
Man	5	1.89	1.81
Man	10	5.86	6.44
Man	20	16.54	20.51
Lu01	5	1.55	1.67
Lu01	10	4.20	5.33
Lu01	20	10.21	14.82
Sent01	5	2.04	1.94
Sent01	10	7.04	7.36
Sent01	20	22.57	25.37

prediction accuracy is high for all images. Thirdly, for QS = 20, MSE can vary in wide range, e.g., from 11.25 for the image "Lu091" to 31.92 for the image "Grass". The predicted values are quite close to the corresponding true ones and, in fact, this takes place for all images employed in our study.

Concerning bias and variance, they are the following: for QS = 5, they are equal to -0.15 and 0.019; for QS = 10 — equal to 0.07 and 0.51; for QS = 20 — equal to to 2.77 and 8.66, respectively. Bias and RMSE are smaller than 16% of mean values for each QS and such an accuracy is acceptable for practice (in fact, PSNR is predicted with maximal error less than 1.4 dB). Comparison of data in Tables 8 and 9 shows that the values of MSE_{pred} for the ADCT coder are usually slightly larger than for the coder AGU. This conclusion can also be drawn from comparison of expressions (7) and (8) where the value of the parameter c is larger in the latter case.

Furthermore, the prediction accuracy for the method [22] using the ADCT coder for QS = 20 has also been analyzed. The minimal predicted MSE is observed for the image "Lu01" (11.63), the maximal (34.43) — for the test image "Grass". The statistical analysis shows that the bias between predicted and true values of MSE is equal to –1.44 and the variance equals to 7.11. This means that prediction accuracy is of the same level as for the method proposed in this paper.

There are several aspects left for discussion. Firstly, all the results presented above have been obtained for non-overlapping blocks fully covering the image area. Thus, for 512 × 512 pixels images used in our analysis, the calculation of $\sigma_{dist}(k), k = 1, \ldots, 4096$ has

Table 9. Comparison of true and predicted MSE values for the ADCT coder for sample images used during the experimental verification.

Image	QS	MSE	MSE_{pred}
A13sm	5	1.84	1.86
A13sm	10	5.46	6.11
A13sm	20	14.85	16.37
Grass	5	2.14	1.99
Grass	10	8.21	7.94
Grass	20	31.92	31.62
Man	5	2.04	1.89
Man	10	6.33	6.85
Man	20	17.39	22.22
Lu01	5	1.69	1.78
Lu01	10	4.61	5.81
Lu01	20	11.25	15.97
Sent01	5	2.09	1.98
Sent01	10	7.39	7.70
Sent01	20	23.63	27.46

been employed. It is possible to expect that the use of overlapping blocks can improve the prediction. Thus, the fully overlapping blocks with their total number equal to $(512-7)\times(512-7) = 255025$ have been additionally used. However, this has not led to an improvement of the prediction accuracy. Moreover, the values of MSE_{pred} corresponding to each other for the non-overlapping and fully overlapping blocks differ insignificantly — by less than 0.04%. For example, for the test image "Fr04" and Q = 20 (the AGU coder) the values of MSE_{pred} are equal to 22.240 and 22.264 for non-overlapping and fully overlapping blocks, respectively. Furthermore, the case when 1000 blocks have been placed randomly has been studied. The obtained prediction results practically do not differ from the corresponding data for non-overlapping blocks. Hence, there are some interesting options for accelerating the prediction by analyzing a limited number of blocks.

Starting from the developed method for predicting MSE, in practice one needs an algorithm for providing a desired value of MSE_{des}. Then, several options can be proposed. For example, as the first step, calculation of a correcting factor as

$$K_{cor} \approx \sum_{k=1}^{K} f^2(\sigma_{im}(k)/\sqrt{12 \cdot MSE_{des}})/K\,, \tag{12}$$

and

$$QS_1 = \sqrt{12 \cdot MSE_{des}/K_{cor}}\,, \tag{13}$$

then determine

$$MSE_1 \approx \sum_{k=1}^{K} \frac{QS_1^2}{12} f^2(\sigma_{im}(k)/QS_1)/K\,. \tag{14}$$

If MSE_1 is quite close to MSE_{des} (e.g., if they differ by no more than 10%), the value $QS_1 = \sqrt{12 \cdot MSE_{des}/K_{cor}}$ may be used for final compression. If this condition is not satisfied, the final QS may be calculated as

$$QS_f = QS_1 \cdot \sqrt{MSE_{des}/MSE_1} \tag{15}$$

and applied for compression.

This algorithm has been first tested for the coder AGU for MSE_{des} = 20 for all twenty images used in previous studies. The provided MSE varies from 11.87 (image "Barbara") to 20.59 (image "Grass"), its bias and variance are equal to 3.22 and 5.79, respectively, hence this accuracy can be considered satisfactory. The final QS varies from 16.04 for the image "Grass" to 24.99 for the image "Frisco", i.e., as expected, the final QS is the largest for

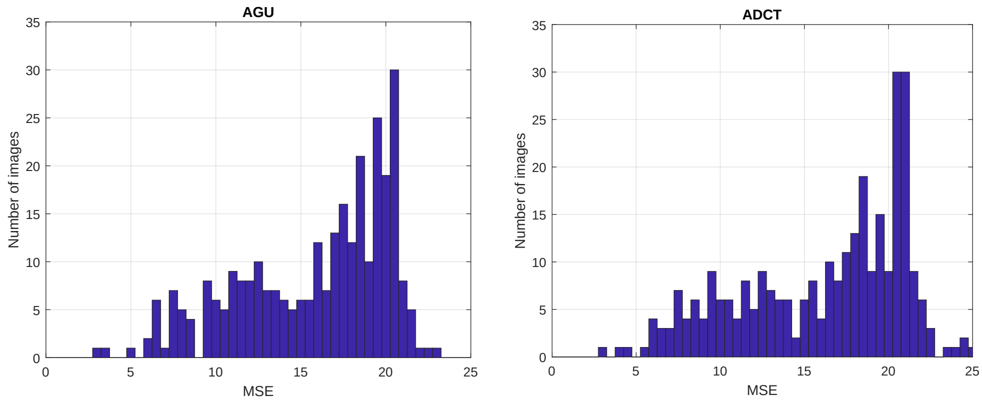

(**a**) (**b**)

Figure 14. Histograms of the provided MSE values obtained for 300 images from TAMPERE17 dataset: (**a**) using AGU coder, (**b**) using ADCT coder.

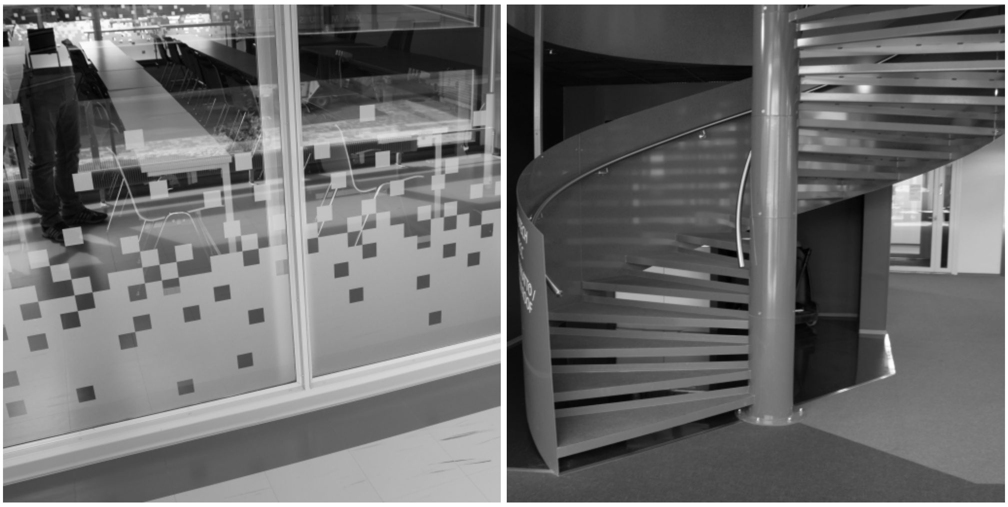

(**a**) (**b**)

Figure 15. Two sample grayscale images from TAMPERE17 dataset with the smallest provided MSE values: (**a**) image no. 257, (**b**) image no. 263.

simple structure images and the smallest for complex structure images. As one can see, the provided MSE are, on average, smaller than desired and this mainly happens for simple structure images. On one hand, this can be useful in practice since one has some "reserve" in quality just for images for which the distortions are more visible. On the other hand, it is possible to introduce some additional correction to remove bias.

The proposed algorithm has been also tested for the ADCT coder for $MSE_{des} = 20$. The provided MSE varies in the limits from 12.06 for the image "Barbara" to 21.16 for the image "San Diego". The bias and variance are equal to 2.86 and 6.46, respectively. So, again bias and RMSE of errors smaller than 15% have been obtained; such an accuracy can be considered satisfactory. The final QS varies in the limits from 16.04 for the image "Grass" to 24.90 for the image "Frisco".

The additional verification of the proposed algorithm has been made for 300 grayscale versions of of 512 × 512 pixels images from the TAMPERE17 noise-free image database [37]. The obtained results for $MSE_{des} = 20$ are presented in the form of histograms for AGU and ADCT coders in Figure 14. In most cases, the provided MSE values are quite close to $MSE_{des} = 20$. Although the provided MSE values are shifted with respect to the desired MSE, and the variance of the final MSE is quite large, an important advantage is that the provided MSE values are mostly smaller than the desired MSE. The smallest provided

MSE are observed for images with a simple and specific structure, e.g., those presented in Figure 15. This phenomenon and its reasons are planned to be investigated in future research.

As it may be seen, the algorithm of determination of the final QS is computationally very simple. It requires the calculation of $\sum_{k=1}^{K} f^2(\sigma_{im}(k)/QS_1)/K$ twice, where the functions $f(\bullet)$ are quite simple, the calculation of $\sigma_{im}, k = 1, \ldots, K$, and elementary comparison and arithmetic operations. Being realized at Intel Core i7 L620 2.00 GHz with 8GB of RAM, they take 0.363$\pm$0.025 seconds for non-overlapping blocks for the image of size 512 $\times$ 512 pixels. Recall here that compression by AGU takes 1.020$\pm$0.040 seconds (whilst decompression requires 1.735$\pm$0.083 seconds). Thus, prediction is sufficiently faster than compression. Note that, additionally, it is possible to use a smaller number of analyzed blocks — if, e.g., 1000 blocks placed randomly are used instead of 4096 non-overlapping blocks, predicted MSEs differ by less than 1%, hence such an approach is appropriate for practice. In this case, prediction can be realized by one order of magnitude less time than compression.

For the ADCT coder the prediction time for non-overlapping blocks is 0.374$\pm$0.065 seconds whilst compression requires 3.080$\pm$0.125 seconds, i.e. prediction and determination of the final QS is considerably faster than compression (decompression requires 1.998$\pm$0.123 seconds). Certainly, prediction can be additionally accelerated compared to the case of non-overlapping blocks by using a smaller number of blocks.

The obtained results have one more positive outcome. They allow proposing the more adequate model (compared to [38]) for simulating distortions due to lossy compression as spatially uncorrelated (white) Gaussian noise with variance dependent on image local activity.

6. Conclusions

In this paper, the statistical and spatial spectral analysis of distortions introduced by two DCT-based coders has been carried out. The cases of visually lossless compression of images and hardly noticeable distortions have been studied. It has been demonstrated that distortions are spatially uncorrelated and their local variance is dependent on image local activity where. It is shown that the distortions' variance is considerably smaller than $QS^2/12$ in locally passive areas. Meanwhile, the local variance of introduced distortions is about $QS^2/12$ for locally active areas, for which $\sigma_{im}/QS \geq 1$.

It is expected that prediction is possible not only for MSE but also for visual quality metrics both full-reference and no-reference ones [39,40]. An extension of the proposed approach for visual quality metrics is one of the directions of further research. Another possibility is the application of some other coders as well as the extension of the proposed approach for video sequences. Additionally, a simple neural network may be implemented that uses QS and a few parameters characterizing image complexity, such as entropy, variance, edge ratio, etc.

The analysis performed has allowed proposing the methodology for predicting MSE that has been intensively tested for images of different origins. It is demonstrated that high accuracy of prediction is provided for two DCT-based coders. The additional advantages of this prediction is its high processing speed. It allows not only predicting MSE, but also calculating QS to be set for a given image to provide a desired MSE.

Author Contributions: Conceptualization, V.L.; methodology, V.L. and K.O.; software, V.A. and S.A.; validation, S.A., S.K. and V.L.; formal analysis, V.A., V.L. and K.O.; investigation, S.K., P.L. and V.L.; resources, S.A. and S.K.; data curation, S.A.; writing—original draft preparation, V.L. and K.O.; writing—review and editing, V.L. and K.O.; visualization, V.A. and P.L.; supervision, V.L.; project administration, V.L. and K.O.; funding acquisition, K.O.

Funding: This research received no external funding.

Institutional Review Board Statement: Not applicable.

Informed Consent Statement: Not applicable.

Data Availability Statement: Not applicable.

Conflicts of Interest: The authors declare no conflict of interest. The funders had no role in the design of the study; in the collection, analyses, or interpretation of data; in the writing of the manuscript; or in the decision to publish the results.

Abbreviations

The following abbreviations are used in this manuscript:

ADCT	Advanced Discrete Cosine Transform
AWGN	additive white Gaussian noise
BPP	bits per pixel
CR	compression ratio
DCT	Discrete Cosine Transform
JPEG	Joint Photographic Experts Group
MOS	Mean Opinion Score
MSE	Mean Square Error
PCC	parameter that controls compression
PSNR	Peak Signal-to-Noise Ratio
QF	quality factor
QS	quantization step
RMSE	Root Mean Square Error
RS	Remote Sensing

References

1. Dutton, W.H. The Social Shaping of Digital Research. *SSRN Electronic Journal* **2012**. https://doi.org/10.2139/ssrn.2019877.
2. George, A.D.; Wilson, C.M. Onboard Processing With Hybrid and Reconfigurable Computing on Small Satellites. *Proceedings of the IEEE* **2018**, *106*, 458–470. https://doi.org/10.1109/jproc.2018.2802438.
3. Christophe, E. Hyperspectral Data Compression Tradeoff. In *Optical Remote Sensing*; Springer Berlin Heidelberg, 2011; pp. 9–29. https://doi.org/10.1007/978-3-642-14212-3_2.
4. Prince, J.L.; Links, J. *Medical Imaging Signals and Systems*; Pearson Higher Education & Professional Group, 2014; p. 544.
5. Bataeva, K. Analysis of advertisement gender images in social-iconographic context. *Actual Problems of Philosophy and Sociology* **2015**, *5*, 15–21.
6. Kiryati, N.; Landau, Y. Dataset Growth in Medical Image Analysis Research. *Journal of Imaging* **2021**, *7*, 155. https://doi.org/10.3390/jimaging7080155.
7. Remote Sensing Services Market by Application, Platform (Satellites, UAVs, Manned Aircraft, Ground), End Use, Resolution (Spatial, Spectral, Radiometric, Temporal), Type, Technology (Active, Passive) and Region - Global Forecast to 2027. Technical report, Research and Markets, 2022.
8. Blanes, I.; Magli, E.; Serra-Sagrista, J. A Tutorial on Image Compression for Optical Space Imaging Systems. *IEEE Geoscience and Remote Sensing Magazine* **2014**, *2*, 8–26. https://doi.org/10.1109/mgrs.2014.2352465.
9. Kaur, R.; Choudhary, P. A Review of Image Compression Techniques. *International Journal of Computer Applications* **2016**, *142*, 8–11. https://doi.org/10.5120/ijca2016909658.
10. Patidar, G.; Kumar, S.; Kumar, D. A Review on Medical Image Data Compression Techniques. In Proceedings of the 2nd International Conference on Data, Engineering and Applications (IDEA). IEEE, 2020. https://doi.org/10.1109/idea49133.2020.9170679.
11. Bondžulić, B.; Stojanović, N.; Petrović, V.; Pavlović, B.; Miličević, Z. Efficient Prediction of the First Just Noticeable Difference Point for JPEG Compressed Images. *Acta Polytechnica Hungarica* **2021**, *18*, 201–220. https://doi.org/10.12700/aph.18.8.2021.8.11.
12. Taubman, D.S.; Marcellin, M. *JPEG2000: Image Compression Fundamentals, Standards and Practice*; The International Series in Engineering and Computer Science, Springer, 2001; p. 800.
13. Zemliachenko, A.; Lukin, V.; Ponomarenko, N.; Egiazarian, K.; Astola, J. Still image/video frame lossy compression providing a desired visual quality. *Multidimensional Systems and Signal Processing* **2015**, *27*, 697–718. https://doi.org/10.1007/s11045-015-0333-8.
14. Bellard, F. BPG image format. Online, 2018. Available at: http://bellard.org/bpg/.
15. Braunschweig, R.; Kaden, I.; Schwarzer, J.; Sprengel, C.; Klose, K. Image Data Compression in Diagnostic Imaging: International Literature Review and Workflow Recommendation. *RöFo - Fortschritte auf dem Gebiet der Röntgenstrahlen und der bildgebenden Verfahren* **2009**, *181*, 629–636. https://doi.org/10.1055/s-0028-1109341.
16. Ieremeiev, O.; Lukin, V.; Okarma, K.; Egiazarian, K.; Vozel, B. On properties of visual quality metrics in remote sensing applications. *Electronic Imaging* **2022**, *34*, 354–1–354–6. https://doi.org/10.2352/ei.2022.34.10.ipas-354.
17. Wang, Z.; Bovik, A.; Sheikh, H.; Simoncelli, E. Image Quality Assessment: From Error Visibility to Structural Similarity. *IEEE Transactions on Image Processing* **2004**, *13*, 600–612. https://doi.org/10.1109/tip.2003.819861.
18. Kassem, A.; Hamad, M.; Haidamous, E. Image compression on FPGA using DCT. In Proceedings of the 2009 International Conference on Advances in Computational Tools for Engineering Applications. IEEE, 2009. https://doi.org/10.1109/actea.2009.5227881.
19. Ponomarenko, N.; Lukin, V.; Egiazarian, K.; Astola, J. DCT Based High Quality Image Compression. In *Image Analysis*; Springer Berlin Heidelberg, 2005; pp. 1177–1185. https://doi.org/10.1007/11499145_119.

20. Ponomarenko, N.; Lukin, V.; Egiazarian, K.; Astola, J. ADCTC: advanced DCT-based coder. In Proceedings of the Proceedings of the 2008 International Workshop on Local and Non-Local Approximation in Image Processing, LNLA2008, Lausanne, Switzerland, 23-24 August 2008; Foi, A.; Gotchev, A., Eds., 2008, p. 6 p.
21. Minguillon, J.; Pujol, J. JPEG standard uniform quantization error modeling with applications to sequential and progressive operation modes. *Journal of Electronic Imaging* **2001**, *10*, 475. https://doi.org/10.1117/1.1344592.
22. Krivenko, S.; Zriakhov, M.; Lukin, V.; Vozel, B. MSE and PSNR prediction for ADCT coder applied to lossy image compression. In Proceedings of the 2018 IEEE 9th International Conference on Dependable Systems, Services and Technologies (DESSERT). IEEE, 2018, pp. 613–618. https://doi.org/10.1109/dessert.2018.8409205.
23. Li, F.; Krivenko, S.; Lukin, V. A Two-step Approach to Providing a Desired Visual Quality in Image Lossy Compression. In Proceedings of the 2020 IEEE 15th International Conference on Advanced Trends in Radioelectronics, Telecommunications and Computer Engineering (TCSET). IEEE, 2020. https://doi.org/10.1109/tcset49122.2020.235483.
24. Krivenko, S.S.; Krylova, O.; Bataeva, E.; Lukin, V.V. Smart Lossy Compression of Images Based on Distortion Prediction. *Telecommunications and Radio Engineering* **2018**, *77*, 1535–1554. https://doi.org/10.1615/telecomradeng.v77.i17.40.
25. Kozhemiakin, R.; Lukin, V.; Vozel, B. Image quality prediction for DCT-based compression. In Proceedings of the 2017 14th International Conference The Experience of Designing and Application of CAD Systems in Microelectronics (CADSM). IEEE, 2017. https://doi.org/10.1109/cadsm.2017.7916121.
26. Vozel, B.; Kozhemiakin, R.A.; Abramov, S.K.; Lukin, V.V.; Chehdi, K. Output MSE and PSNR prediction in DCT-based lossy compression of remote sensing images. In Proceedings of the Image and Signal Processing for Remote Sensing XXIII; Bruzzone, L.; Bovolo, F.; Benediktsson, J.A., Eds. SPIE, 2017. https://doi.org/10.1117/12.2278002.
27. Chopra, A.; Sharma, S.; Kadyan, V. Need of green computing to improve environmental condition in current era. In Proceedings of the 2016 International Conference on Electrical, Electronics, and Optimization Techniques (ICEEOT). IEEE, 2016. https://doi.org/10.1109/iceeot.2016.7755296.
28. Li, F.; Lukin, V.; Ieremeiev, O.; Okarma, K. Quality Control for the BPG Lossy Compression of Three-Channel Remote Sensing Images. *Remote Sensing* **2022**, *14*, 1824. https://doi.org/10.3390/rs14081824.
29. Abramova, V.; Lukin, V.; Abramov, S.; Abramov, K.; Bataeva, E. Analysis of Statistical and Spatial Spectral Characteristics of Distortions in Lossy Image Compression. In Proceedings of the 2022 IEEE 2nd Ukrainian Microwave Week (UkrMW). IEEE, 2022. https://doi.org/10.1109/ukrmw58013.2022.10036949.
30. Wallace, G. The JPEG still picture compression standard. *IEEE Transactions on Consumer Electronics* **1992**, *38*, xviii–xxxiv. https://doi.org/10.1109/30.125072.
31. Pearlman, W.; Islam, A.; Nagaraj, N.; Said, A. Efficient, Low-Complexity Image Coding With a Set-Partitioning Embedded Block Coder. *IEEE Transactions on Circuits and Systems for Video Technology* **2004**, *14*, 1219–1235. https://doi.org/10.1109/tcsvt.2004.835150.
32. Ponomarenko, N.; Lukin, V.; Astola, J.; Egiazarian, K. Analysis of HVS-Metrics' Properties Using Color Image Database TID2013. In *Advanced Concepts for Intelligent Vision Systems*; Springer International Publishing, 2015; pp. 613–624. https://doi.org/10.1007/978-3-319-25903-1_53.
33. Ponomarenko, N.; Silvestri, F.; Egiazarian, K.; Carli, M.; Astola, J.; Lukin, V. On between-coefficient contrast masking of DCT basis functions. In Proceedings of the Proceedings of the Third International Workshop on Video Processing and Quality Metrics for Consumer Electronics, VPQM 2007, Scottsdale, Arizona, USA, 25-26 January 2007, 2007, p. 4 p. Contribution: organisation=sgn,FACT1=1.
34. Aiazzi, B.; Alparone, L.; Baronti, S.; Lastri, C.; Selva, M. Spectral Distortion in Lossy Compression of Hyperspectral Data. *Journal of Electrical and Computer Engineering* **2012**, *2012*, 1–8. https://doi.org/10.1155/2012/850637.
35. Abramova, V.V.; Abramov, S.K.; Lukin, V.V. Iterative Method for Blind Evaluation of Mixed Noise Characteristics on Images. *Information and Telecommunication Sciences* **2015**, *0*, 8–14. https://doi.org/10.20535/2411-2976.12015.8-14.
36. Abramova, V.; Abramov, S.K.; Lukin, V.V.; Roenko, A.A.; Vozel, B. Automatic estimation of spatially correlated noise variance in spectral domain for images. *Telecommunications and Radio Engineering* **2014**, *73*, 511–527. https://doi.org/10.1615/telecomradeng.v73.i6.40.
37. Ponomarenko, M.; Gapon, N.; Voronin, V.; Egiazarian, K. Blind estimation of white Gaussian noise variance in highly textured images. *Electronic Imaging* **2018**, *30*, 382–1–382–5. https://doi.org/10.2352/issn.2470-1173.2018.13.ipas-382.
38. Li, F.; Lukin, V.; Proskura, G.; Vasilyeva, I.; Chernova, G. Image Classification Accuracy Analysis for Three-channel Remote Sensing Data. In Proceedings of the Proceedings of the 3rd International Workshop on Intelligent Information Technologies & Systems of Information Security (IntellTSIS 2022), Khmelnytskyi, Ukraine, March 23–25, 2022; Hovorushchenko, T.; Savenko, O.; Popov, P.; Lysenko, S., Eds., 2022, Vol. 3156, *CEUR Workshop Proceedings*, pp. 505–519.
39. Liu, J.; Zhou, W.; Li, X.; Xu, J.; Chen, Z. LIQA: Lifelong Blind Image Quality Assessment. *IEEE Transactions on Multimedia* **2022**, pp. 1–16. https://doi.org/10.1109/tmm.2022.3190700.
40. Zhu, H.; Li, L.; Wu, J.; Dong, W.; Shi, G. MetaIQA: Deep Meta-Learning for No-Reference Image Quality Assessment. In Proceedings of the 2020 IEEE/CVF Conference on Computer Vision and Pattern Recognition (CVPR). IEEE, 2020. https://doi.org/10.1109/cvpr42600.2020.01415.